ResearchGate

See discussions, stats, and author profiles for this publication at: https://www.researchgate.net/publication/323230540

Bionanocomposite scaffolds based on chitosan–gelatin and nanodimensional bioactive glass particles: In vitro properties and in vivo bone regeneration

Article *in* Journal of Biomaterials Applications · February 2018

DOI: 10.1177/0885328218759042

CITATIONS
49

READS
339

6 authors, including:

Cristian Covarrubias
University of Chile
55 PUBLICATIONS **990** CITATIONS
SEE PROFILE

Monserrat Cádiz
University of the Andes (Chile)
5 PUBLICATIONS **61** CITATIONS
SEE PROFILE

Miguel Ignacio Maureira Vargas
University of Chile
12 PUBLICATIONS **149** CITATIONS
SEE PROFILE

Felipe Cuadra
University of Chile
4 PUBLICATIONS **73** CITATIONS
SEE PROFILE

Some of the authors of this publication are also working on these related projects:

Project U-Redes: Nanomateriales para aplicaciones biológicas View project

Project Aumento de longevidad de restauraciones plásticas View project

All content following this page was uploaded by Miguel Ignacio Maureira Vargas on 16 October 2018.

The user has requested enhancement of the downloaded file.

Check for updates

Hard Tissues and Materials

JOURNAL OF biomaterials applications

Journal of Biomaterials Applications
0(0) 1–9
© The Author(s) 2018
Reprints and permissions:
sagepub.co.uk/journalsPermissions.nav
DOI: 10.1177/0885328218759042
journals.sagepub.com/home/jba
SAGE

Bionanocomposite scaffolds based on chitosan–gelatin and nanodimensional bioactive glass particles: In vitro properties and in vivo bone regeneration

Cristian Covarrubias, Monserrat Cádiz, Miguel Maureira, Isabel Celhay, Felipe Cuadra and Alfredo von Marttens

Abstract

Bone repair bionanocomposite scaffolds were produced by incorporating dense bioactive glass nanoparticles or mesoporous bioactive glass nanospheres into a chitosan–gelatin polymer blend. The in vitro bioactivity of the scaffolds was assessed in simulated body fluid, and cell viability and osteogenic differentiation assays were performed with dental pulp stem cells. Bone regeneration properties of the scaffold materials were in vivo assessed by using a critical-sized femoral defect model in rat. The scaffold nanocomposites showed excellent cytocompatibility and ability to accelerate the crystallization of bone-like apatite in vitro. Bionanocomposites prepared with bioactive glass nanoparticles were particularly more active to promote the osteogenic differentiation of dental pulp stem cells as judged by the higher activity of alkaline phosphatase. This result is attributed to the faster dissolution of bioactive glass nanoparticles into osteogenic ionic products compared to mesoporous bioactive glass nanospheres. In vivo experiments demonstrated that bioactive glass nanoparticles (5%)/chitosan–gelatin bionanocomposite significantly produces the highest amount of new bone (~80%) in the defect area after eight weeks of implantation. The bone regeneration capacity exhibited by the scaffolds formulated with nanodimensional bioactive glass particles make them attractive for bone reconstruction applications.

Keywords

Bioactive glass nanoparticles, bionanocomposite scaffold, chitosan, gelatin, bone regeneration

Introduction

Bioactive glass (BG) is a material well-known for its properties to stimulate bone tissue repair.[1] This resorbable and osteoproductive material promotes bone-tissue formation on its surface, and it bonds to surrounding living tissue when implanted in the body. The commercial BG-based products contain particles with micrometer dimensions that are produced through high-temperature melting process. Nowadays, advances in nanomaterial science enable the synthesis of BG with nanometric particle size, controlled nanostructures, and using relatively low temperatures through sol–gel techniques. Essentially dense BG nanoparticles (nBG) are produced with a particle size in the range of 30–90 nm,[2] while BG nanospheres with a highly ordered hexagonal arrangement of mesoporous (nMBG) can be synthesized by incorporating supramolecular chemistry to the sol–gel process.[3] In previous work, our group systematically studied the effect of the nanoscale structure of BG particles on their in vitro bioactivity and capacity to osteogenically differentiate stem cells.[4] The results demonstrate that the nanometric particle size of BG is a more determining factor on its in vitro osteogenic properties than the nanoporous structure, being nBG and nMBG the most promissory particles. These bioactive nanopowders, however, require being appropriately processed for their use in bone reconstruction applications.

Laboratory of Nanobiomaterials, ICOD, Faculty of Dentistry, University of Chile, Santiago, Chile

Corresponding author:
Cristian Covarrubias, Universidad de Chile, Sergio Livingstone 943, Independencia, Santiago de Chile 1025000, Chile.
Email: ccovarrubias@odontologia.uchile.cl

Alveolar bone augmentation procedures preferably demand materials with improved surgical handling and moldable characteristics.[5] Bionanocomposites prepared by incorporating bioactive ceramic nanoparticles into biodegradable polymeric matrices are interesting materials that combine the bioactivity of nanoparticles with the supporting and flexibility properties of a three-dimensional polymeric matrix (scaffold).[6,7] Although nanocomposite scaffolds based on hydroxyapatite, tricalcium phosphate, and calcium phosphate cements particles have been extensively reported,[8] crystalline bioceramics commonly exhibit lower bioactivity and a slower rate of apatite formation than bioglasses.[9] Likewise, many synthetic and natural polymers have been used in the attempt to produce scaffolds. Although synthetic polymers enable to fabricate scaffolds with a tailored architecture, they have drawbacks including the risk of rejection due to reduced bioactivity.[10] Unlike synthetic polymers, natural polymers are biologically active, promote improved cell adhesion and growth, and exhibit excellent biodegradability. We have formulated a chitosan–gelatin (ChGel) polymer blend with excellent properties for scaffold fabrication; mainly because it is formulated with a non-toxic cross-linker.[11] So, it is expected that the incorporation of nanodimensional BG particles into ChGel matrix leads to scaffold biomaterials with improved osteostimulative properties. In the current study, we present the preparation and bioactive properties of nanocomposite scaffolds based on ChGel matrix loaded with BG nanoparticles. Bionanocomposites with nBG and nMBG were produced, structurally characterized, and their biological properties assessed by in vitro and in vivo experiments.

Materials and methods

Preparation of scaffold bionanocomposites

nBG (~70 nm) and nMBG (~100 nm) nanoparticles were synthesized by the sol–gel method using the procedures and molar compositions reported in our previous work.[4] nBG/ChGel and nMBG/ChGel nanocomposites containing a weight ratio of Ch/Gel of 1:1 and with 5% and 25% w/w nanoparticle content were prepared. For this purpose, a chitosan solution was prepared by dissolving 4 g of chitosan (high molecular weight, >75%–85% deacetylated, Sigma-Aldrich) in 100 mL of 1% lactic acid. Appropriate amounts of dried nanoparticle powder were added to 100 mL of 4% w/w aqueous gelatin (bovine skin type B, Sigma-Aldrich) solution and dispersed by sonication for 20 min. After that, nanoparticle/gelatin dispersion was mixed with chitosan solution under stirring using a vertical paddle mixer. The hydrogel blend was crosslinked by adding 30 mL of a solution of sodium hexametaphosphate (M & B Ltd.) and sodium hydroxide (Merck) dissolved in 100 mL of distilled water with a weight ratio of 0.3:4. Scaffolds were prepared individually placing 1 mL of nBG/ChGel or nMBG/ChGel crosslinked-gel into 48 well plates. The samples were frozen at −80°C for 24 h and then freeze-dried for two to three days at −45°C using an FD5518 freeze dryer (ILShineBioBase Co. Ltd.) to obtain sponge nanocomposites. Neat ChGel sponges were also prepared as a control.

In vitro bioactivity assays

The ability of the bionanocomposites to induce the formation of apatite was assessed in a cellular simulated body fluid (SBF), which has inorganic ion concentrations similar to those of human extracellular fluid. The SBF solution was prepared as described by Kokubo et al.,[12] using the standard ion composition (Na^+ 142.0, K^+ 5.0, Mg^{2+} 1.5, Ca^{2+} 2.5, Cl^- 147.8, HCO_3^- 4.2, HPO_4^{2-} 1.0, and SO_4^{2-} 0.5 mM). The fluid was buffered at physiological pH 7.4 at 37°C with tri-(hydroxymethyl) aminomethane and hydrochloric acid. The cylindrical bionanocomposites samples (1.0 cm × 0.5 cm) were individually soaked in 50 mL of SBF in polyethylene containers at 36.5°C using a thermostatic bath. After incubation for seven days, the scaffolds were removed from SBF, rinsed with distilled water, and dried at 60°C.

Material characterization

The structure of scaffold bionanocomposites and apatite formation was analyzed by scanning electron microscopy (SEM), equipped with X-ray dispersive energy elemental microanalysis (EDX) in a JEOL model JSM-IT300LV microscope. Pore size distribution was measured analyzing SEM Images magnified 40 times a scale of 500 μm by ImageJ v1.44 Software (NIH). Apatite formation was also analyzed by X-ray diffraction (XRD) on a Siemens D, 5000 diffractometer using CuKa radiation within a 2θ range of 5°–50° at a scanning speed of 1.2°/min. The chemical structure of the materials was characterized by total attenuated reflectance with Fourier transform infrared spectroscopy (ATR-FTIR) using an Agilent Cary 630 ATR-FTIR spectrometer.

Cell culture

Stem cells isolated from dental pulp (DPSCs) were used to evaluate cell proliferation and differentiation. DPSCs were isolated from healthy third molars extracted at the orthodontist's recommendation after obtaining informed consent from the patients and

ethics approval from the Ethics Committee of the Faculty of Dentistry of University of Chile. DPSCs were cultured in Dulbecco's modified Eagle medium (Alpha-MEM; Invitrogen Life Technologies) contained 10% fetal bovine serum (FBS GIBCO), 100 U/mL penicillin, and 100 µg/mL streptomycin; 10,000 cells were seeded directly into 10×8 mm cylindrical scaffolds placed in a single well of a 48-well cell culture plate (1.6×10^4 cells per cm^3 of scaffold volume). Cell viability was determined at 3, 7, and 14 days of incubation by using the CellTiter 96® AQueous One Solution Cell Proliferation Assay (Promega), which measures the reduction of [3–(4,5-dimethylthiazol-2-yl)-5–(3-carboxymethoxyphenyl)-2–(4-sulfophenyl)-2H- tetrazolium] (MTS) to formazan by mitochondria in viable cells. The activity of the alkaline phosphatase (ALP) enzyme of DPSCs cultured with the scaffolds was determined by the colorimetric dephosphorylation assay of the p-nitrophenyl phosphate reagent, which was followed by measuring the absorbance with an Infinite F-50 microplate reader (Tecan) at 405 nm at 3, 7, and 14 days of incubation.

In vivo studies

Surgical implantation

In vivo experiments were conducted in a total of eight Sprague-Dawley adult rats, according to the codes and rules of the Ethics Committee of the Faculty of Medicine of University of Chile (Protocol CBA #0542 FMUCH), taking care of surgical procedures, pain control, standards of living, and appropriated death.

The effect of scaffold nanocomposites on early bone regeneration was evaluated using a rat femoral model. Rats were anesthetized with ketamine and xylazine previous to the surgical procedure. The region of the surgery was shaved and disinfected. A critical-sized defect of 4 mm was created in the rat femoral mid-diaphysis using a diamond-trephine of 4 mm in diameter under saline irrigation. Defects were treated randomly with

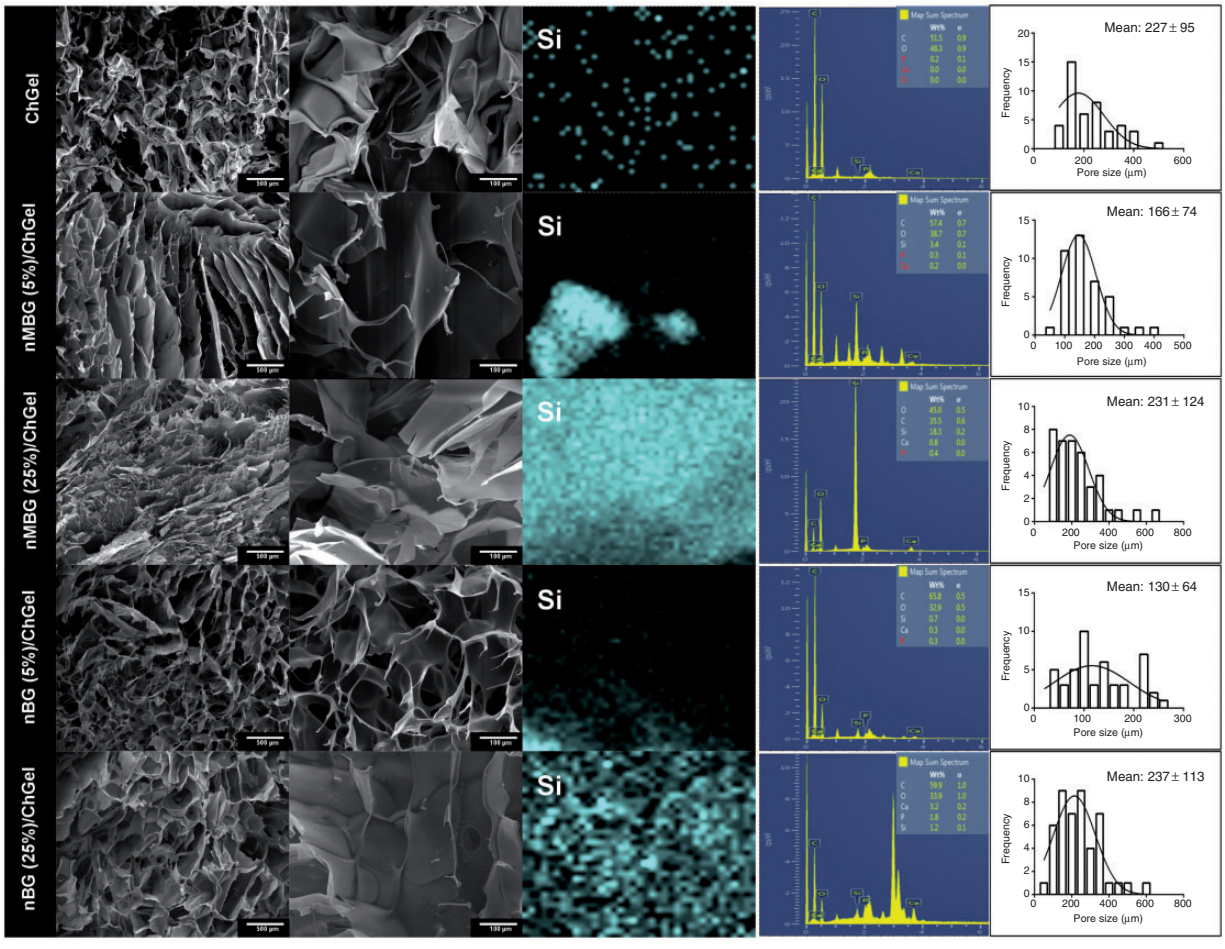

Figure 1. SEM images, EDX elemental analysis and pore size distribution of ChGel, nMBG/ChGel, and nBG/ChGel bionanocomposite scaffolds.

ChGel, nBG (5%)/ChGel, nMBG (5%)/ChGel, or left untreated (Control). After eight weeks, the animals were sacrificed by CO_2 inhalation, and the bone defect sites were harvested for subsequent evaluation.

Histological analysis

The bone samples were fixed in 10 wt. % formaldehyde for 48 h and then immersed in ascending concentrations of ethanol (Winkler). Samples were then embedded in epoxy resin without decalcification. The embedded blocks were cut with a low-speed diamond blade saw (SYJ-150, MTI Corporation) to obtain 200 μm discs in thickness.

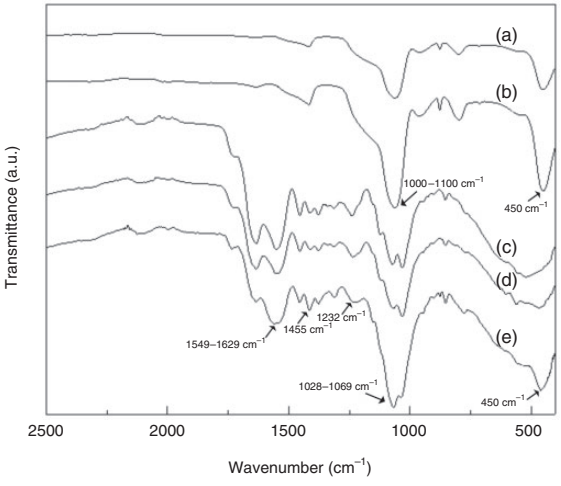

Figure 2. ATR-FTIR spectra of nMBG (a), nBG (b), ChGel (c), nMBG (25%)/ChGel (d), and nBG (25%)/ChGel (e).

The tissue sections were Au sputter-coated in a Desk V Sputter Coater (Denton Vacuum Inc.) at 7.27×10^{-2} Torr and 45 mA for 30 s and examined with scanning electron microscopy in back-scattered electron mode (BSE-SEM) using a JEOL IT300LV microscope. The observations were performed at an accelerating voltage of 20 kV and a working distance of 23.6 mm. BS-SEM images obtained at ×20 magnification were used to measure the bone area by using the ImageJ software. The percentage of newly formed bone (NB) was calculated according to the following equation:

NB (%) = (area of newly formed bone in the 4 mm diameter defect/total area of the 4 mm diameter defect) × 100.

Tissue specimens were also analyzed by X-ray computed microtomography (Micro-CT) in a Bruker Micro-CT Skyscan 1278. Micro-CT images were acquired at 50 μm resolution (voltage: 59 kV, current: 537 μA, 1.0 mm Al filter, rotation step: 0.25). The raw data acquired were reconstructed using NRecon Software (Skyscan, Belgium). The 3D images of the bone defects were generated using CTAn v.1.12 software (Bruker-microCT) and visualized by 3D CTVox (Bruker-microCT).

Statistical analysis

Data were analyzed employing one-way analysis of variance with post hoc multiple comparisons achieved using Tukey's test by using GraphPad prism 6 (GraphPad Software, San Diego, CA). A minimum

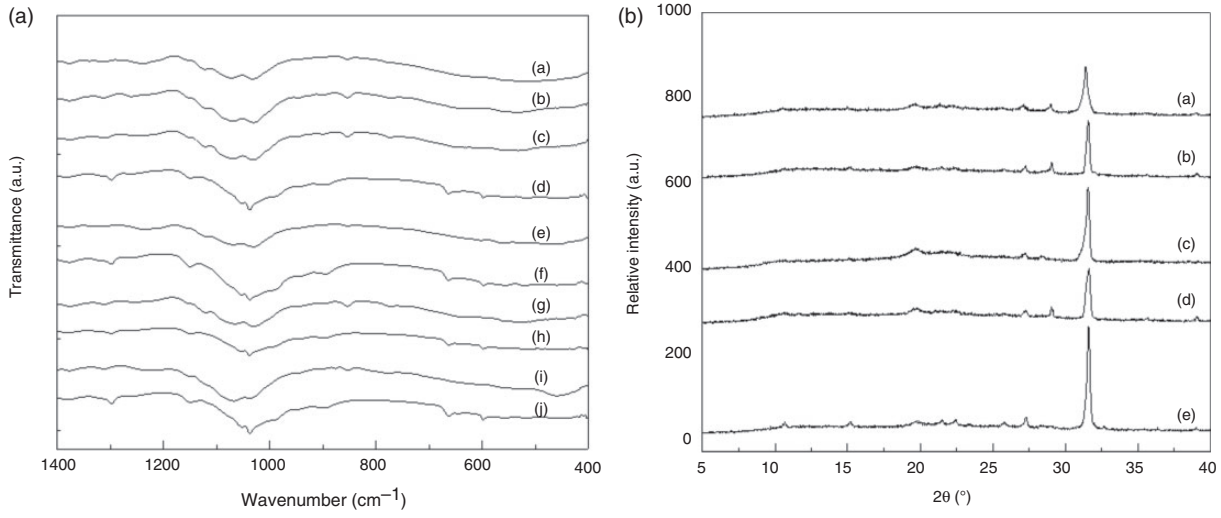

Figure 3. (A) ATR-FTIR spectra of scaffold materials before and after to be conditioned in SBF at 36.5°C for 7 days. ChGel – before SBF (a), ChGel – 7 days SBF (b), nMBG(5%)/ChGel – before SBF (c), nMBG(5%)/ChGel – 7 days SBF (d), nMBG(25%)/ChGel – before SBF (e), nMBG(25%)/ChGel – 7 days SBF (f), nBG(5%)/ChGel – before SBF (g), nBG(5%)/ChGel – 7 days SBF (h), nBG (25%)/ChGel – before SBF (i), and nBG (25%)/ChGel – 7 days SBF (j). (B) XRD pattern of ChGel – 7 days SBF (a), nMBG(5%)/ChGel – 7 days SBF (b), nMBG(25%)/ChGel – 7 days SBF (c), nBG(5%)/ChGel – 7 days SBF (d), and nBG (25%)/ChGel – 7 days SBF (j).

of $n = 3$ was used and $p < 0.05$ was admitted statistically significant.

Results and discussion

Figure 1 shows SEM images, EDX elemental analysis, and pore size distribution of neat ChGel scaffold and those of the nanocomposites prepared with BG nanoparticle. Porosity of neat scaffold and nanocomposites produced with nBG adopted a relatively regular morphology, while pores of nanocomposites prepared with nMBG are more elongated in shape. Moreover, mean pore size of scaffold loaded with 5% wt (~148 µm) tended to be smaller than those with 25% nanoparticle

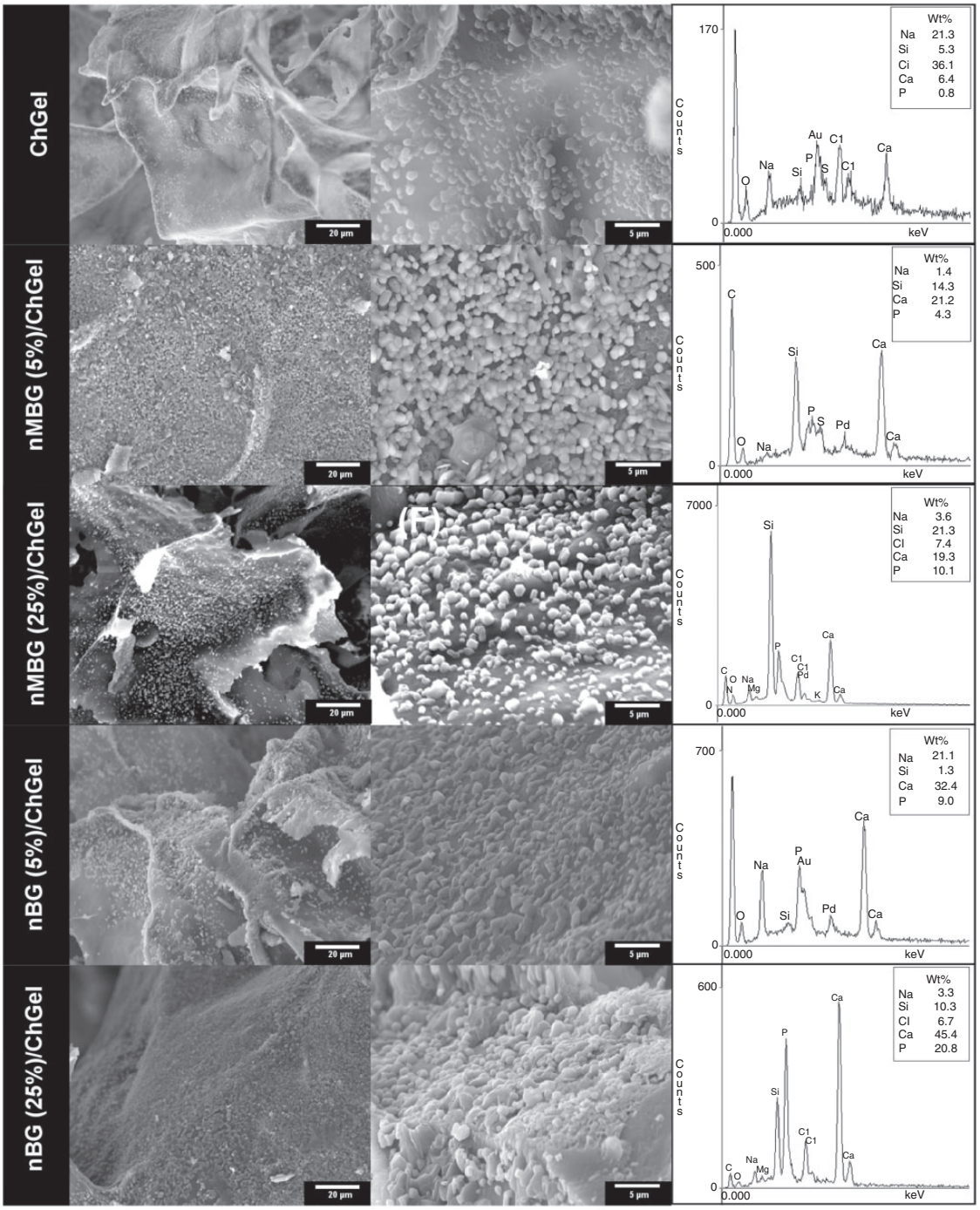

Figure 4. SEM images and EDX elemental analysis of the surface of ChGel, nMBG/ChGel, and nBG/ChGel bionanocomposite scaffold after immersion in SBF for seven days.

content (~234 μm). Nanoparticle incorporation may affect the mechanism of pore formation from ice crystal templates. It has been found that different sizes and types of nanoparticles can induce different instability in the ice front,[13] nanoparticle surface energy can also cause unusual ice-nanoparticle segregation behavior or induce other ice structures; affecting thus the size and shape of the pores.[14] Compositional analysis performed by EDX shows contents of Ca, P, and Si related with the presence of BG nanoparticles into the polymer matrix. Particularly, Si mapping suggests a relatively uniform distribution of the BG particles into the polymer. The nanoparticles and scaffold materials were also analyzed by ATR-FTIR (Figure 2). Spectra of BG nanoparticles exhibit bands at 450 cm^{-1} and, 1060 cm^{-1} corresponding to Si-O-Si bending mode of their siliceous structure, while neat ChGel scaffold spectrum present peaks at 1028–1069, 1232, 1455, and 1549–1629 cm^{-1} corresponding to the characteristic vibrations of amide and amine groups of chitosan and gelatin structures.[15,16] Although no evident covalent interactions between the nanoparticles and functional groups of the polymer matrix were detected, the Si-O-Si vibration at 450 cm^{-1} in the nanocomposite spectra confirm the presence of the BG nanoparticles incorporated into the ChGel matrix.

The ability of the nanocomposite scaffolds to induce the formation of bone-like apatite on its surface was assessed in SBF at seven days of incubation. The evolution of apatite formation on the scaffold surfaces analyzed by ATR-FTIR and XRD (Figure 3). Spectra of nanocomposites immersed in SBF shows the presence of bands at 595 cm^{-1} and 660 cm^{-1}, assigned to the P-O bending vibration and another strong band around, 1040 cm^{-1}, attributed to the P-O symmetric stretching vibration in crystalline apatite.[17] These apatite vibrations were not detected in the neat scaffold. However, XRD analysis confirmed the formation of apatite on both the neat scaffold and nanocomposites as judged by the presence of the most characteristic apatite peak at 31.7°, corresponding to the 211 reflection of the apatite crystal (JCPD 205166). SEM examination revealed the presence of the mineral phase on the scaffold surfaces (Figure 4). EDX analysis shows that these precipitates are constituted mainly of calcium and phosphorus elements. A higher degree of mineralization in terms of density, extension, and cluster mineral size can be seen on the bionanocomposite scaffolds. Particularly, bionanocomposite filled with 25% nBG exhibits a denser apatite layer that almost completely covered its surface. nBG nanoparticles have shown to have a higher dissolution rate in SBF than nMBG[4] which promotes more rapid apatite crystallization and explains the higher degree of mineralization

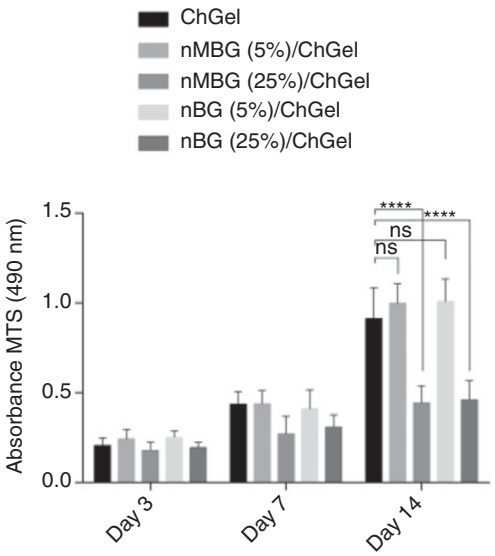

Figure 5. Viability of DPSCs cultured in the presence of the ChGel, nMBG/ChGel, and nBG/ChGel bionanocomposite scaffolds at different culture times as determined by the MTS assay.

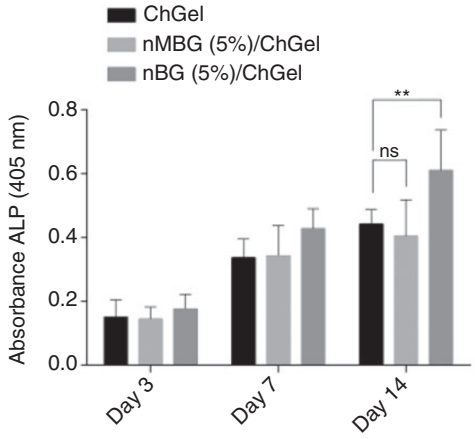

Figure 6. ALP activity in DPSCs cultured at different times with ChGel, nMBG/ChGel, and nBG/ChGel bionanocomposite sacffolds in the absence of osteogenic supplements.

observed on the nBG (25%)/ChGel bionanocomposite surface.

Cytocompatibility of the scaffold materials was assessed using DPSCs until 14 days of incubation (Figure 5). MTS absorbance values of mitochondrial activity of cells cultured with the bionanocomposites for seven days did not present differences with respect to those grown on the neat ChGel scaffold. At 14 days of incubation, cell viability is maintained on both nBG and nMBG 5% bionanocomposites, while it statistically decreased when cultured on the 25% bionanocomposites. Bionanocomposites with high nanoparticle loading may generate high calcium concentrations

from BG dissolution that reduce the cell proliferation, as has been observed by Valerio et al.[18] Based on the cytocompatibility properties, bionanocomposite scaffolds loaded with 5% of BG nanoparticles were chosen for further biological testing. The ability of the scaffolds to stimulate the osteogenic differentiation of DPSCs was assessed by quantifying the expression of ALP enzyme (Figure 6), which is produced when bone forming cells lay down the bone extracellular matrix.[19] Statistically, significant higher ALP activity values were measured on the nBG (5%)/ChGel nanocomposite at 14 days of culture. Through BG ionic dissolution products, stem cells can chemically drive along the osteoblastic pathway, resulting in increased mineralizing activity.[20] It has been demonstrated that specific concentrations of ionic dissolution products of BG recreate an extracellular environment that is capable of supporting osteoblast phenotype expression and extracellular matrix deposition and bone nodule mineralization in osteoblasts.[21] In a previous work,[4] we demonstrated that nBG nanoparticles in powder form have higher capacity to stimulate the ALP expression than nMBG. Higher external surface area of nBG nanoparticles enables a fast glass dissolution compared with the internal and less accessible surface area provided by the MBG nanoporous structure. The results of the current study show that nBG retains in vitro superior bioactivity even when the nanoparticles are constituent of a composite scaffold material.

The in vivo bone repair potential of the scaffold biomaterials was assessed in a rat femur defect. Figure 7 shows the bone defect area analyzed by BS-SEM, EDX, and Micro-CT after eight weeks of implantation. In BS–SEM images, mineralized areas are shown as brighter zones, while soft tissues are seen in darker color. It can be observed that both the neat scaffold and bionanocomposites were able to stimulate new bone formation. BS-SEM results are consistent with the density and distribution of calcium atoms as well as with the three-dimensional

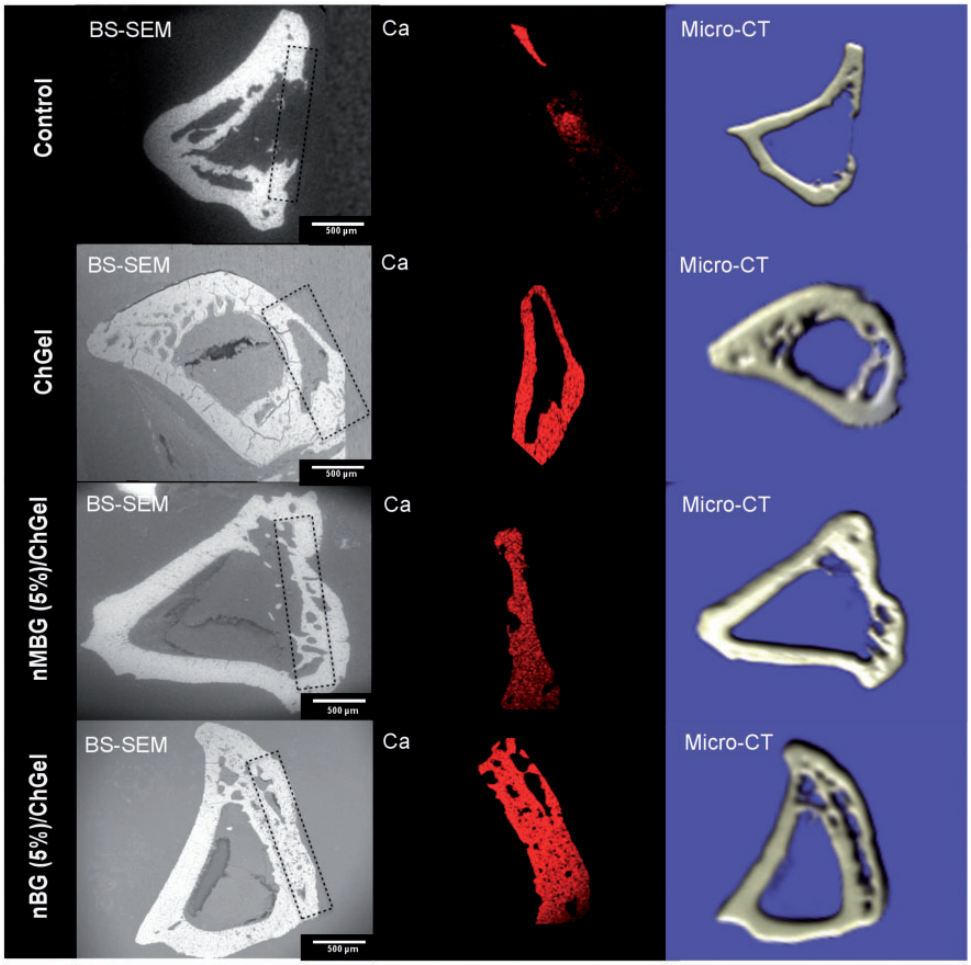

Figure 7. Bone defect area analyzed by BS-SEM, EDX-calcium mapping, and Micro-CT after eight weeks of implantation.

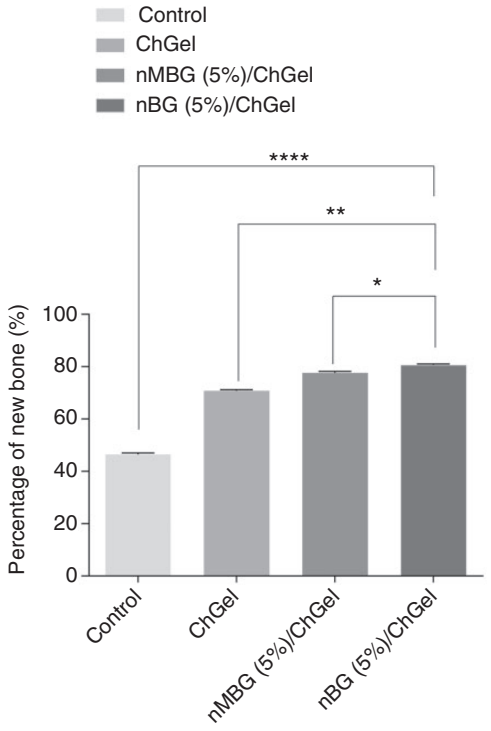

Figure 8. Percentage of new bone formed in the untreated defect (control) and in those treated with the scaffolds after eight weeks of implantation.

reconstruction of the bone defect area performed by micro-CT. Figure 8 confirms that scaffold biomaterials have significantly greater percent bone than the untreated control group ($p < 0.01$). The capacity of neat ChGel scaffold to stimulate bone regeneration can be attributed to Arg-Gly-Asp (RGD)-like sequence in gelatin structure, which promotes cell attachment to the scaffolds via focal adhesion.[22,23] Moreover, chitosan forms ionic complexes with negatively charged gelatin that affect the polycationic interaction of chitosan with the anionic cell surface, which has been reported to influence the tissue remodeling process.[24] From Figure 8, it can also be seen that defect treated with nBG (5%)/ChGel significantly generated the greatest amount of new bone (~80%) over all other groups. The results of the current study demonstrate that the in vivo osteogenic capacity of ChGel scaffold is significantly enhanced with the incorporation of BG nanoparticles. To our best knowledge, this is the first report of the in vivo bone regeneration properties of ChGel bionanocomposite scaffolds prepared with nanodimensional nBG or nMBG particles. As already discussed and investigated in previous works, high rate of dissolution of nanosized BG particles into osteogenic ionic products accelerates of bone formation processes. The improved osteogenic properties of BG nanoparticles combined with bioactivity and supporting properties of the ChGel polymer matrix make bionanocomposites promissory materials to accelerate the bone reconstruction treatments.

Conclusions

Nanostructured nBG and nMBG particles were combined with a ChGel polymer matrix to produce bionanocomposite scaffolds. The nanocomposite materials showed excellent cytocompatibility and ability to induce the crystallization of bone-like apatite in vitro. Bionanocomposites prepared with nBG nanoparticles were particularly more active to promote the osteogenic differentiation of stem cells as judged by the higher activity of ALP. In vivo implantation of the scaffolds into bone defect model demonstrated that nBG (5%)/ChGel bionanocomposite significantly produces the greatest amount of new bone. The bone regeneration capacity exhibited by the bionacomposite scaffolds formulated with nanodimensional BG particles make them attractive to be assessed for bone reconstruction in future clinical trials.

Declaration of Conflicting Interests

The author(s) declared no potential conflicts of interest with respect to the research, authorship, and/or publication of this article.

Funding

The author(s) disclosed receipt of the following financial support for the research, authorship, and/or publication of this article: This work was supported by ENLACE project (ENL008/16), Vice presidency of Research and Development (VID), University of Chile.

References

1. Jones JR. Review of bioactive glass: from Hench to hybrids. *Acta Biomater* 2012; 9: 4457–4486.
2. Zheng K and Boccaccini AR. Sol-gel processing of bioactive glass nanoparticles: a review. *Adv Colloid Interface Sci* 2017; 249: 363–373.
3. Izquierdo-Barba I and Vallet-Regí M. Mesoporous bioactive glasses: relevance of their porous structure compared to that of classical bioglasses. *Biomed Glas* 2015; 1: 140–150.
4. Covarrubias C, Arroyo F, Balanda C, et al. The effect of the nanoscale structure of nanobioceramics on their *in vitro* bioactivity and cell differentiation properties. *J Nanomater* 2015; 2015: 1–14.
5. Ibrahim MS, El-Wassefy NA and Farahat DS. Biocompatibility of dental biomaterials. In L Tayebi and K Moharamzadeh (eds) *Biomaterials for Oral and*

Dental Tissue Engineering. Duxford: Woodhead Publishing, 2017, pp.117–140.
6. Gloria A, De Santis R and Ambrosio L. Polymer-based composite scaffolds for tissue engineering. *J Appl Biomater Biomech* 2010; 8: 57–67.
7. Meskinfama M, Bertoldia S, Albanesea N, et al. Polyurethane foam/nano hydroxyapatite composite as a suitable scaffold for bone tissue regeneration. *Mater Sci Eng: C* 2018; 82: 130–140.
8. Yunos DM, Bretcanu O and Boccaccini AR. Polymer-bioceramic composites for tissue engineering scaffolds. *J Mater Sci* 2008; 43: 4433–4442.
9. Hench LL. Bioceramics. *J Am Ceram Soc* 1998; 81: 1705–1728.
10. Shoichet MS. Polymer scaffolds for biomaterials applications. *Macromolecules* 2010; 43: 581–591.
11. Gupta KC and Jabrail FH. Controlled-release formulations for hydroxy urea and rifampicin using polyphosphate-anion-crosslinked chitosan microspheres. *J Appl Polym Sci* 2007; 104: 1942–1956.
12. Kokubo T, Kushitani H, Sakka S, et al. Solutions able to reproduce in vivo surface-structure changes in bioactive glass-ceramic A-W3. *J Biomed Mater Res A* 1990; 24: 721–734.
13. Rohatgi PK and Adams CM. Effect of freezing rates on dendritic solidification of ice from aqueous solutions. *Trans Metall Soc AIME* 1967; 239: 1729–1736.
14. Ehre D, Lavert E, Lahav M, et al. Water freezes differently on positively and negatively charged surfaces of pyroelectric materials. *Science* 2010; 327: 672–675.
15. El-Hefian EA, Nasef M, Yahaya AH, et al. Preparation and characterization of chitosan/agar blends: rheological and thermal studies. *J Chil Chem Soc* 2010; 55: 130–136.
16. Hermanto Sumarlin LO and Fatimah W. Differentiation of bovine and porcine gelatin based on spectroscopic and electrophoretic analysis. *J Food Pharm Sci* 2013; 1: 68–73.
17. Hench LL and Wilson J. *An introduction to bioceramics*. 2nd ed. London: Imperial College Press, 2013, pp. 530–531.
18. Valerio P, Pereira MM, Goes AM, et al. The effect of ionic products from bioactive glass dissolution on osteoblast proliferation and collagen production. *Biomaterials* 2004; 25: 2941–2948.
19. Blair HC, Larrouture QC, Li Y, et al. Osteoblast differentiation and bone matrix formation *in vivo* and *in vitro*. *Tissue Eng Part B Rev* 2017; 23: 268–280.
20. Bielby RC, Christodoulou IS, Pryce RS, et al. Time- and concentration-dependent effects of dissolution products of 58s sol–gel bioactive glass on proliferation and differentiation of murine and human osteoblasts. *Tissue Eng* 2004; 10: 1018–1026.
21. Sigkou O, Jones JR, Polak JM, et al. Differentiation of fetal osteoblasts and formation of mineralized bone nodules by 45S5 Bioglass conditioned medium in the absence of osteogenic supplements. *Biomaterials* 2009; 21: 3542–3550.
22. Aronow MA, Gerstenfeld LC, Owen TA, et al. Factors that promote progressive development of the osteoblast phenotype in cultured fetal rat calvaria cells. *J Cell Physiol* 1990; 143: 213–221.
23. Thein-Han WW, Saikhun J, Pholpramoo C, et al. Chitosan–gelatin scaffolds for tissue engineering: physico-chemical properties and biological response of buffalo embryonic stem cells and transfectant of GFP–buffalo embryonic stem cells. *Acta Biomater* 2009; 5: 3453–3466.
24. Huang Y, Onyeri S, Siewe M, et al. In vitro characterization of chitosan–gelatin scaffolds for tissue engineering. *Biomaterials* 2005; 26: 7616–7627.

View publication stats